Mitigation of Oscillations in Switching Frequency-Based Active Thermal Control

Riccardo Sancio, *Student Member, IEEE*, Martin Votava, Karthik Debbadi, *Student Member, IEEE*, Yoann Pascal, and Marco Liserre, *Fellow, IEEE*

***Abstract*—Power electronics modules are highly susceptible to thermal cycling stress during operation, which can significantly reduce their lifespan. Active thermal control (ATC) techniques are deployed to mitigate this stress and enhance module longevity. Among the various ATC strategies, switching frequency-based active thermal control (SF-ATC) is the simplest and most commonly used to suppress the junction temperature variation, reducing the accumulated damage. However, this method can lead to oscillations and instability in the switching frequency, which can negatively impact both the power converter operation and the ATC performance. While solutions to mitigate oscillations have been proposed, the issue of instability has not been adequately addressed in the literature. This study presents a comprehensive analytical and Simulink-based simulation and investigation of the switching frequency instability in SF-ATC. Furthermore, a modification of the classic SF-ATC is proposed to mitigate oscillations and instability. The proposed SF-ATC aims to enhance the overall ATC performance in terms of thermal swing reduction and limit the impact on the converter operation (e.g., power quality). The effectiveness of the proposed method is then experimentally validated.**

***Index Terms*—Active thermal control (ATC), instability, reliability, switching frequency, thermal management.**

I. Introduction

POWER semiconductor devices are susceptible to thermal cycling stress over their lifetime. The different thermal expansions of the packaging components (such as direct bond copper substrates and wire bonds) may cause mechanical stress-related problems due to the thermal cycling that the power module undergoes during operation.

Received 11 April 2025; revised 11 June 2025; accepted 4 July 2025. Date of publication 10 July 2025; date of current version 27 August 2025. This work was supported in part by the Interreg Deutschland-Danmark with funds from the European Regional Development Fund via the Smart Power Con- version project under Grant 16-2, 1-221 and in part by the Kopernikus Project ENSURE 'New ENergy grid StructURes for the German Energiewende' under Grant 03SFK1I0-2. Recommended for publication by Associate Editor K. Ngo. *(Corresponding author: Riccardo Sancio.)*

Riccardo Sancio and Martin Votava are with the Chair of Power Electronics, Kiel University, 24143 Kiel, Germany (e-mail: risa@tf.uni-kiel.de; mvo@tf.uni-kiel.de).

Karthik Debbadi and Yoann Pascal are with Fraunhofer-Institut für Siliziumtechnologie ISIT, 25524 Itzehoe, Germany (e-mail: karthik.debbadi@isit.fraunhofer.de; yoann.pascal@isit.fraunhofer.de).

Marco Liserre is with the Chair of Power Electronics, Kiel University, 24143 Kiel, Germany, and also with Fraunhofer-Institut für Siliziumtechnologie ISIT, 25524 Itzehoe, Germany (e-mail: marco.liserre@isit.fraunhofer.de).

Color versions of one or more figures in this article are available at https://doi.org/10.1109/TPEL.2025.3587071.

Digital Object Identifier 10.1109/TPEL.2025.3587071

As a solution, Murdock et al. [1] introduced the concept of active thermal control (ATC), which aims to reduce damage by mitigating the thermal swing (ΔT_j) through the manipulation of variables which have effect on the semiconductor power dissipation (e.g., gate control modification strategies [2], [3], modulation strategy [4], and switching frequency [5], [6]). As a result, the topic of ATC is growing with the introduction of various damage reduction strategies [7], [8]. Among the possible control variables, the main advantages of using the switching frequency-based active thermal control (SF-ATC) to suppress the thermal swing are the ease of implementation on commercially available microcontroller units, the absence of hardware modification (low cost burden), and the limited impact on the converter operating point. During SF-ATC application, a variation of switching frequency of the power converter is provided to temporarily boost the dies power losses and reduce the thermal swing. The main limitation of switching frequency manipulation for reducing converter damage is its impact on power quality and EMI propagation. While higher switching frequencies improve current waveform quality, they also lead to EMI issues. To mitigate this, switching frequency variation should be limited [6]. However, excessively narrow variations render SF-ATC ineffective. Therefore, the switching frequency range must balance SF-ATC performance with compliance to EMI and power quality standards [9]. In the context of the control strategy adopted for the SF-ATC, although the use of a reference junction temperature trajectory can yield to achieve robust and precise control of the junction temperature [10], [11], [12], [13], [14], [15], [16], satisfactory thermal stress relief performance is achievable with reference-free ATC solutions when working within the device allowable power losses limitations [6], [17], [18], [19]. In this case, the control input is represented by the estimated semiconductor power losses variation (ΔP_{loss})-based on high-pass filtering. Subsequently, based on the control input, an algorithm calculates the required control variable variation (e.g., Δf_{sw}) to compensate the temperature change. In [17], [18], and [19], the switching power losses (SLPF) are manipulated by increasing the switching frequency during the decreasing current phase of the load profile in order to level out the junction temperature. Nevertheless, these solutions may present fast oscillating switching frequency variations due to imperfect averaging of power losses, noise affecting the current measurement (required to estimate power losses) and high control algorithms gains. These fast oscillations cause a decrease in the overall system performance, increased EMI, higher noise

propagation and audible noise. To cope with this problem, the use of an hysteresis band-based algorithm to suppress the abrupt switching frequency transitions has been proposed in [20], [21], [22], [23], and [24]. In these works, the switching frequency (output) and power losses (input) variation range is divided in different thresholds and a change of the output is obtained only if the input increases or decreases over or below one of these set thresholds hence creating dead-band zones where no change in switching frequency occurs. Another possible solution is to embed an additional low-pass filter (LPF) unit in the switching frequency modulation loop [13].

However, despite these solutions proved to be effective in suppressing smaller switching frequency oscillations, they can degrade the SF-ATC performance in terms of the thermal swing suppression. Moreover, these solutions do not address the potential issue of the switching frequency instability in SF-ATC techniques.

This work is the first to propose a thorough mathematical study of the switching frequency instability in SF-ATC strategies. In addition, this work proposes to modify the classic SF-ATC controller, presented in [17], [18], and [19], to achieve the maximal ATC stress relief while suppressing fast switching frequency oscillations. The experimental validation is carried out to prove the effectiveness of the proposed method.

The rest of this article is organized as follows. In Section II, the basic principle of the SF-ATC is described, while the switching frequency instability problem is introduced and analyzed. Moreover, the LPF action and hysteresis band method are applied to evaluate their effectiveness in reducing the switching frequency oscillations. The proposed method is presented in Section III, while Section IV describes the adopted experimental setup and investigates the switching frequency instability experimentally. In addition, here, the experimental evaluations for each of the solutions are provided for a comparison in terms of switching frequency dynamics, thermal swing reduction, and accumulated damage reduction. In Section V, a discussion on the main work contribution, future research work and applicability of the method is presented. Finally, Section VI concludes this article.

II. Problem Identification and Analysis

In this section, the fundamental concept of the reference-free SF-ATC is examined, and the issue of switching frequency instability is presented. Furthermore, the application of traditional solutions for reducing switching frequency oscillations is analyzed.

A. Switching Frequency-Based ATC

The SF-ATC working principle is briefly described as follows. During operation, each IGBT die experiences conduction P_{cond} and SLPF P_{sw}. The power losses estimation is obtained by

$$P_{\text{cond}} = V_{\text{ce}}(T_{\text{j}}, i_{\text{out}})\, i_{\text{out}}\, \alpha \quad \text{and}$$
$$P_{\text{sw}} = f_{\text{sw}} \underbrace{\left(E_{\text{on}}(T_{\text{j}}, i_{\text{out}}, V_{\text{dc}}) + E_{\text{off}}(T_{\text{j}}, i_{\text{out}}, V_{\text{dc}})\right)}_{E_{\text{sw}}} \quad (1)$$

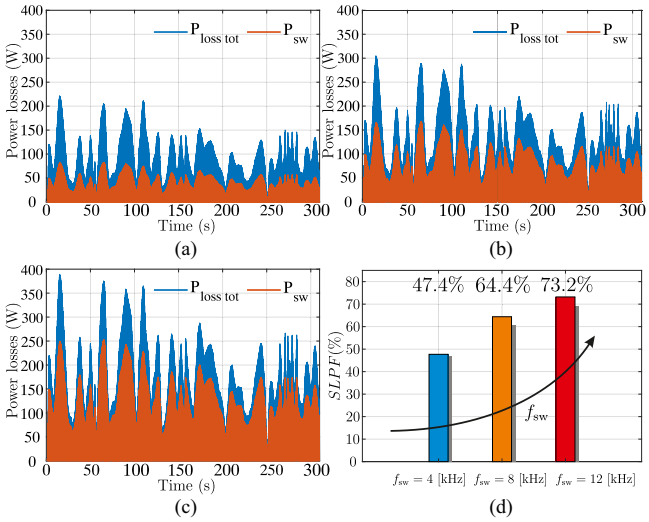

Fig. 1. SLPF impact over the total power losses amount during a generic load profile for (a) $f_{\text{sw}} = 4$ kHz; (b) $f_{\text{sw}} = 8$ kHz; and (c) $f_{\text{sw}} = 12$ kHz. (d) Shows the percent SLPF participation factor SLPF for the different switching frequencies.

where V_{ce} is the collector–emitter voltage drop during the ON-state, α is the duty cycle, f_{sw} the switching frequency, E_{on} and E_{off} the turn-ON and turn-OFFenergy losses, respectively, V_{dc} is the dc-link voltage, i_{out} is load current averaged on the switching period of the die, and T_{j} is the die junction temperature information, which can be either measured or estimated. The energies as well as the collector–emitter voltage drop are calculated by means of lookup tables (LUTs) based on the power module datasheet information. If the total power losses P_{loss} are described in normalized form, then the participation factor for conduction power losses (CLPF) and the SLPF can be defined as in

$$P_{\text{loss}} = P_{\text{cond}} + P_{\text{sw}} \rightarrow 1 = \text{CLPF} + \text{SLPF with}$$
$$\text{CLPF} = \frac{P_{\text{cond}}}{P_{\text{loss}}}, \quad \text{SLPF} = \frac{P_{\text{sw}}}{P_{\text{loss}}}. \quad (2)$$

Fig. 1(a)–(c) demonstrates the contribution of an IGBT die SLPF over the chip total power losses for a generic load profile and different switching frequencies. As shown, the SLPF increases as the switching frequency increases. This is further confirmed in Fig. 1(d) where the same participation factor is integrated over the entire load profile. The SF-ATC dynamically adjusts the switching frequency to boost the switching power dissipation, ensuring it reaches levels where the participation factor SLPF is sufficiently high (SLPF $\geq 50\,\%$) to influence the die temperature and mitigate thermal swings. Fig. 2 shows the reference-free SF-ATC block diagram for a single die (IGBT) device. As depicted, no junction temperature reference trajectory is generated. The measured data from the power module (e.g., dc link voltage, duty cycle, phase currents, etc.) and the information on the junction temperature T_{j} are used to calculate the conduction and switching losses by interpolation of the power module datasheet information.

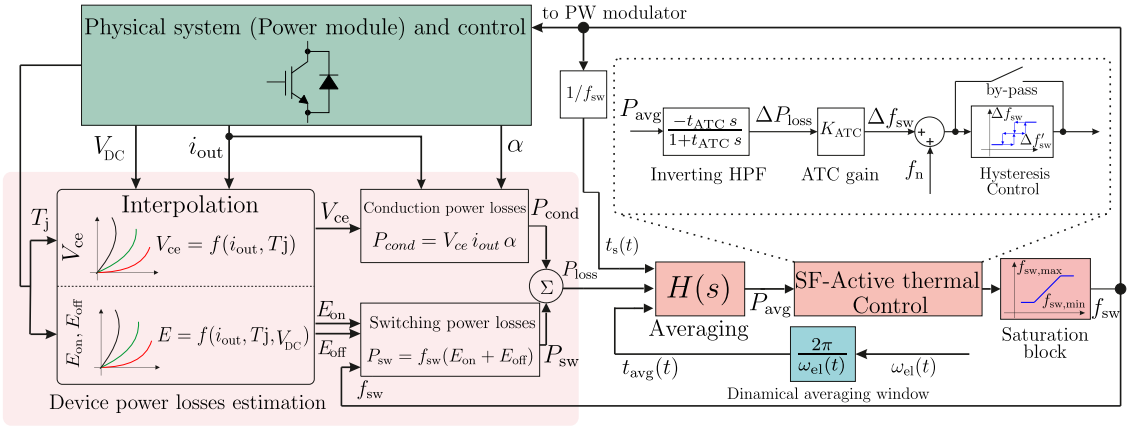

Fig. 2. General SF-ATC block diagram (for a single IGBT die).

The total power losses P_{loss} are then calculated and averaged over a current fundamental period P_{avg}. Subsequently, the SF-ATC algorithm converts the power losses information into the necessary switching frequency f_{sw} value to reduce the thermal swing. This is done by using an inverting high-pass filter (IHPF) to compute the variation of the averaged power losses ΔP_{loss} and amplify it by using an ATC gain K_{ATC}. The switching frequency is updated as the sum of the base value f_n and the computed variation Δf_{sw}. The updated switching frequency f_{sw} is eventually sent to the SLPF computation block to update the power losses value as well as to the pulsewidth modulation register to be applied to the real physical dies (see Fig. 2).

The power losses averaging $H(s)$ is deployed by a dynamical moving average filter with

$$N_{\text{s}}(t) = \text{round}\left(\frac{t_{\text{avg}}(t)}{t_{\text{s}}(t)}\right) \tag{3}$$

where N_{s} is the number of processed samples, t_{avg} is the variable average time window which is, in turn, changing based on the electric frequency ω_{el}, while t_{s} is the variable sampling period, changing with the updated switching frequency f_{sw}.

In addition, the switching frequency is bounded by the lower limit $f_{\text{sw,min}}$ to avoid excessive deterioration of power quality, and by the upper limit $f_{\text{sw,max}}$ set according to the studied power module physical limitations.

It should be pointed out that the SF-ATC can have stress relieving effects on both long-term (with a time range of hours) and short-term (with a time range of minutes and seconds) thermal cycles. As such, the choice between these two effects will influence the IHPF time-constant t_{ATC} tuning. However, in the case where long-term thermal cycles are suppressed, the related dies power losses would be excessively increased, severely compromising the efficiency. As such, the second thermal cycles typology are usually addressed.

In the context of the design, the high nonlinearity of the SF-ATC and the unpredictability of the converter load profile represent the two main challenges. However, a preliminary design can be performed on a representative load profile by a systematic exploration of the parameters defined by the pairs $(K_{\text{ATC}}, t_{\text{ATC}})$. For example, the load profile for which the power losses in Fig. 1 were calculated was used to provide a preliminary design of the SF-ATC main parameters. In the analysis, it is assumed $V_{\text{dc}} = 400$ V, nominal frequency $f_{\text{g}} = 50$ Hz, max and min switching frequencies $f_{\text{max}} = 20$ kHz and $f_{\text{min}} = 5$ kHz, respectively. The model has been built in Simulink according to the block diagram in Fig. 2 and the following assumptions:

1) The converter processes pure active power (unitary power factor).
2) The aging impact on the power losses and thermal model parameters is not taken into account in the analysis.
3) The used thermal model for a single IGBT die is retrieved by Andresen et al. [25] for the same power module under study (FP25R12KE3 from Infineon).
4) Thermal cross-coupling effects between the dies are neglected.
5) Only fast thermal cycles (in the range of few seconds to one minute) are addressed, considering a load profile based on a modified version of the worldwide harmonized light vehicles test cycle (WLTC) profile.
6) As the thermal cycles duration of interest are far below the thermal constant of a realistic heatsink, the case temperature is assumed to be constant (20°C).
7) The computation of ON-state voltage drop V_{ce} and switching energies E_{sw} for the power losses estimation is obtained by quadratic interpolation, based on the datasheet information, of the die junction temperature T_{j}, dc-link voltage V_{dc}, and load current i_{out}.

An indication of the SF-ATC performance for a single IGBT die is depicted in Figs. 3 and 4. In particular, Fig. 3 presents the SF-ATC thermal swing reduction capability. As performance index the normalized sum of the junction temperature swing over all the cycles is selected assuming as base the case without ATC ($\Sigma\Delta T_j = 1$ p.u.). Whereas, Fig. 4 illustrates the impact of the ATC on the chip power losses. The findings allow for a preliminary design of the SF-ATC algorithm. In fact, the user can select the parameters based on the desired tradeoff between efficiency and thermal swing reduction.

However, it should be observed that, the selection of an high K_{ATC} may be the preferred option in scenarios where the power module is close to its end-of-life or when there is interest in an

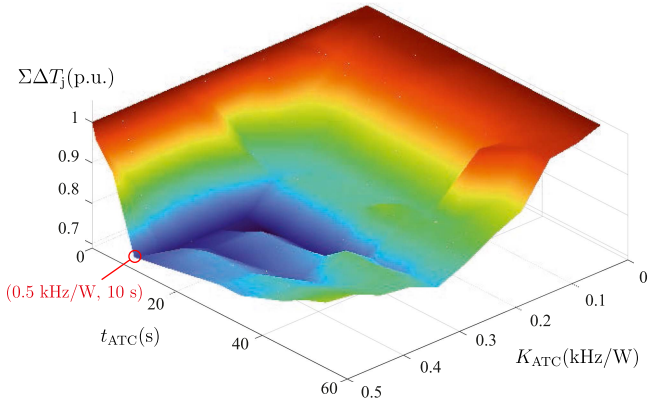

Fig. 3. Example of SF-ATC tuning for maximal thermal cycling reduction in a single die application.

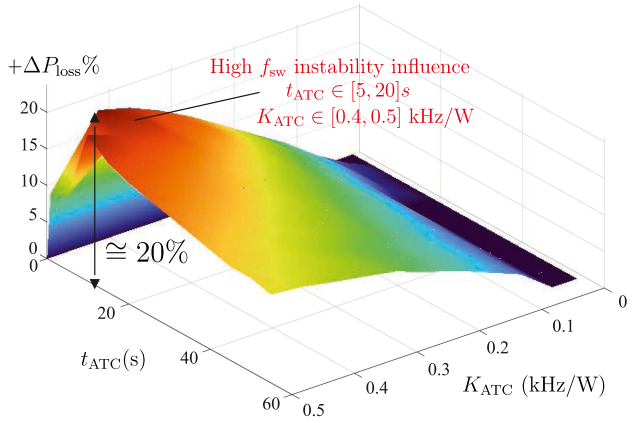

Fig. 4. Impact on a single IGBT die power losses for different values of $(K_{\text{ATC}}, t_{\text{ATC}})$ explored space.

intensive delay of the maintenance for the used power module (e.g., installments in remote and hard to reach locations, such as offshore wind power converters [8]).

For the presented example, the set of parameters that allow for the maximal reduction of thermal stress are $K_{\text{ATC}} = 0.5$ kHz/W and $t_{\text{ATC}} = 10$ s. As reported in Figs. 3 and 4, these lead to a reduction of temperature cycles as high as 30% and to an increase of the single chip power losses higher than 20%.

The peak in the increase of power losses (red region in Fig. 4) is due to the fact that for parameters in the ranges $t_{\text{ATC}} \in [5, 20]$ s and $K_{\text{ATC}} \in [0.4, 0.5]$ kHz/W, the switching frequency instability phenomenon arises, impacting the power losses and the ATC performance, as further confirmed by the simulated evaluation of a portion of the used profile with $t_{\text{ATC}} = 5$ s and $K_{\text{ATC}} = 0.1$–0.5 kHz/W in Fig. 5. As depicted, the increase in ATC gain reflects a boost in the thermal swing suppression, but introduces high oscillations in the switching frequency, further increasing the die power losses. This may lead the designer to opt for higher IHPF time constants. However, this would severely degrade the efficiency since, in this case, also thermal cycles with longer periods would interact with the controller (it is worth to remind that only fast cycles are included in the profile used for simulation).

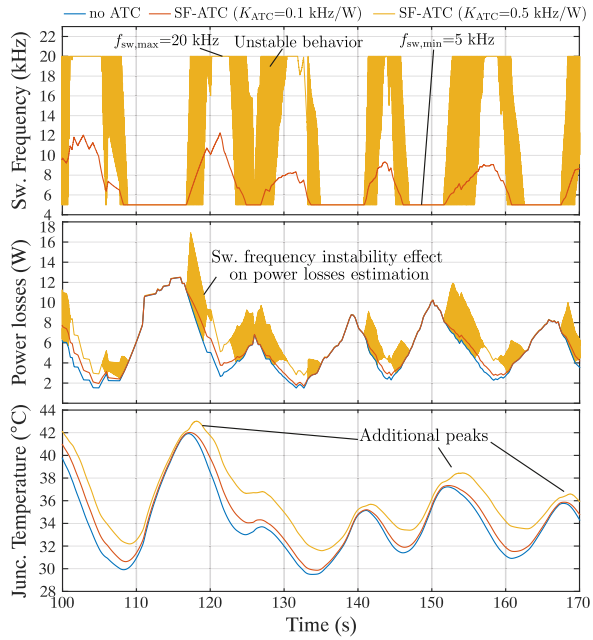

Fig. 5. Portion of the simulation-based evaluation for the impact of SF-ATC design parameters on switching frequency (top), single die power losses (center), and junction temperature fluctuations (bottom) behavior ($t_{\text{ATC}} = 5$ s).

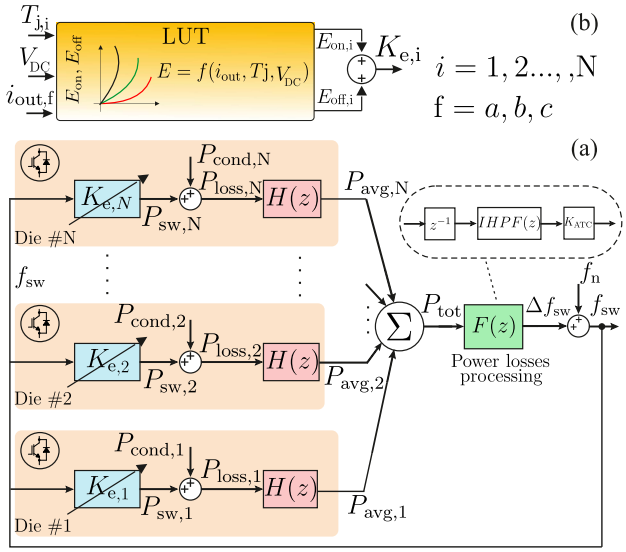

Fig. 6. Study on switching frequency instability. (a) Switching frequency modulation scheme for a three-phase converter application. (b) Each switching energy is assumed as a variable gain based on the interpolation of the DC-link voltage, ith-die junction temperature and load current.

B. Switching Frequency Instability

As the practical application of the SF-ATC is obtained in digital systems and to provide a more detailed analysis of the instability phenomenon, the frequency modulation scheme is represented in the Z-domain transform [see Fig. 6(a)].

From Fig. 2, it can be observed that the calculation of the switching energy losses of the single chips is carried out regardless of the switching frequency. As such, it can be assumed that each die switching energy behaves as a variable gain which value

is obtained from the LUTs based on current, dc-link voltage and junction temperature information [see Fig. 6(b)] $E_{\text{sw,i}} = K_{\text{e,i}}$ with $i = 1, \ldots N$ where N stands for the total number of chips under investigation.

From Fig. 6, the switching frequency output is described by

$$f_{\text{sw}}(z) = f_{\text{n}} + \Delta f_{\text{sw}} = f_{\text{n}} + P_{\text{tot}}(z)\ F(z) \tag{4}$$

where Δf_{sw} is the enabled switching frequency variation provided by the SF-ATC, P_{tot} is the sum of the averaged power losses, f_{n} represents the switching frequency base value and $F(z)$ is the power losses processing transfer function, involving the inverting high-pass filtering IHPF(z), the ATC gain K_{ATC}, and a single-step delay z^{-1}, added to prevent the algebraic loop. Finally, the switching frequency information is used to reupdate the SLPF value by the product of the single chips switching energy and the modulated switching frequency (feedback of the SLPF).

As such, the update of the switching frequency is obtained by

$$f_{\text{sw}}(z) = f_{\text{n}} + K_{\text{ATC}}\ \text{IHPF}(z)\ z^{-1}\ P_{\text{tot}}(z). \tag{5}$$

The Z-domain transfer function of the IHPF is expressed by

$$\text{IHPF}(z) = \frac{-t_{\text{ATC}}\ z + t_{\text{ATC}}}{(t_{\text{ATC}} + t_{\text{s}})\ z + (t_{\text{s}} - t_{\text{ATC}})} \tag{6}$$

being, as mentioned, t_{ATC} the selected ATC filter time constant and t_{s} the sampling time. Involving the single chips power losses computation, it results

$$P_{\text{tot}}(z) = H(z)\ \left(\sum_{i=1}^{N} P_{\text{cond,i}}(z) + f_{\text{sw}}(z)\ \sum_{i=1}^{N} K_{\text{e,i}}\right) \tag{7}$$

where the total switching energy gain is $K_{\text{e,tot}} = \sum_{i=1}^{N} K_{\text{e,i}}$, the global conduction losses are gathered in $d(z) = \sum_{i=1}^{N} P_{\text{cond,i}}$ and $H(z)$ being the average block transfer function, expressed in the Z-domain.

For sake of simplicity, in the following analysis it will be assumed that the averaging is processed with a constant number of samples N_{s} which transfer function is

$$H(z) = \frac{\sum_{i=1}^{N_s} z^{N_s - i}}{N_s\ z^{N_s - 1}}. \tag{8}$$

It can be now observed that the system represented in Fig. 6 is linear thus the superposition principle can be used to derive the desired output $f_{\text{sw}}(z)$. As the main instability phenomenon is related to the SLPF computation loop, the contribution of conduction losses may be neglected ($d(z) = 0$). If (7) is substituted into (5) then solving with respect to the output switching frequency leads to the overall input–output transfer function $G_u(z)$

$$f_{\text{sw}}(z) = G_u(z) f_{\text{n}} = \frac{1}{1 - K_{\text{ATC}}\ z^{-1}\ \text{IHPF}(z)\ H(z)\ K_{\text{e,tot}}} f_{\text{n}}. \tag{9}$$

Considering that the thermal transients are much slower than the sampling process ($t_{\text{ATC}} >> t_{\text{s}}$) and that the switching frequency oscillations occur in high frequency ranges, the effect of the IHPF transfer function is negligible in the frequency range of the instability [i.e., IHPF$(z) \simeq -1$].

TABLE I
SIMULATION PARAMETERS

Parameter and measure unit	Value
K_{ATC}, ATC slope gain (kHz/W)	0.5
N_{s}, number of samples	10
t_{ATC}, HPF time constant (s)	10
V_{dc}, dc-link voltage (V)	400
$f_{\text{sw,max}}$, max. switching frequency (kHz)	30
$f_{\text{sw,min}}$, min. switching frequency (kHz)	4
N_{hyst}, number of hysteresis steps	5
$K_{\text{e,tot lim}}$, limit global energy gain (mJ)	20

By defining the global loop gain $K_{\text{tot}} = \frac{K_{\text{ATC}}\ K_{\text{e,tot}}}{N_{\text{s}}}$, (9) can be rewritten as

$$G_u(z) = \frac{z^{N_{\text{s}}}}{z^{N_{\text{s}}} + K_{\text{tot}}\ \sum_{i=1}^{N_s} z^{N_s - i}}. \tag{10}$$

If K_{tot} exceeds unity the system becomes unstable, with the poles of (10) migrating outside the stability circle (see Fig. 7, based on data from Table I).Starting by the stability limit condition ($K_{\text{tot}} = 1$), the related energy threshold that guarantees the SF-ATC stability is computed as

$$K_{\text{e,tot lim}} = \frac{N_{\text{s}}}{K_{\text{ATC}}}. \tag{11}$$

Using the parameters provided in Table I, the simulation conducted in the Simulink environment is carried out based on the model reported in Fig. 6 when considering the case $N_{\text{s}} = 10$. As reported, the stability threshold is calculated to be 20 mJ. The instability of the switching frequency occurs when the global energy value $K_{\text{e, tot}}$ is higher than the computed threshold $K_{\text{e,tot lim}}$. Although the switching frequency is expected to diverge, the saturation block maintains the oscillation within the two bounds, while the stable switching frequency states are reached as the total energy falls below $K_{\text{e,tot lim}}$. It is worth mentioning that, in this example, mission profiles and parameter values are chosen to provide the best observation of the transition between stable and unstable switching frequency behavior. Assuming a constant current injection of 106 A_{rms}, the effect of instability on the load phase current due to the introduced fast frequency oscillation is reported in Fig. 8(a), while the same current without the switching frequency oscillations is shown in Fig. 8(b). The fast Fourier transform is applied to the current period and the result is shown in Fig. 9. The instability introduces spectral components in the ATC selected switching frequency range, having negative impact on the power quality. As a consequence, the overall system efficiency is decreased due to higher load losses and additional EMI issues are introduced.

C. LPF and Hysteresis Band Methods

To evaluate the hysteresis bands impact on the switching frequency oscillations, the simulation conducted based on the model of Fig. 6 has been repeated in the case of an hysteresis band block with $N_{\text{hyst}} = 5$ in the modality illustrated in Fig. 2 (with open bypass switch in the ATC section). During stable conditions, the use of hysteresis bands eliminates the switching frequency oscillations, as shown in Fig. 7(a) (center). However,

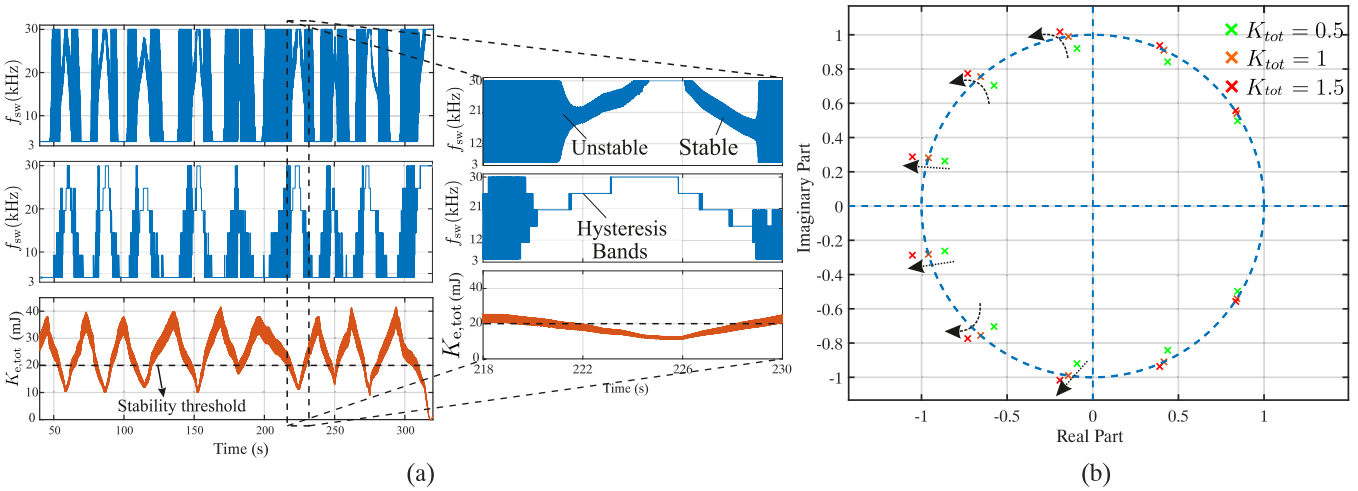

Fig. 7. Simulation evaluation of the switching frequency instability phenomena. (a) Dynamics evaluated during the application of a generic mission profile in simulation environment (upper) and during hysteresis band application (center), during the variation of the global estimated switching energy $K_{\mathrm{e,tot}}$ (bottom). (b) Pole-zero map showing how the poles of (10) tend to exit the stability circle for global system gains over unity.

it is not effective in suppressing the oscillations in the case of switching frequency instability.

On the other hand, Fig. 10 illustrates the two possible options for using an LPF to eliminate switching frequency oscillations. The first option is to embed an LPF into the switching frequency loop, while the second option is to use an external LPF action. The use of an external LPF action is not convenient as, in this case, the filtered switching frequency signal is not used to update the power losses value, resulting in a larger error between the estimated and actual junction temperature when estimators are used.

While, despite the use of an internal LPF action in the switching frequency modulation loop [option (a)] can smooth the switching frequency behavior, this comes at the expense of a reduced ATC effectiveness, depending on the amplitude and slope of the load current. Thus, when considering the LPF action, it is important to note that its ability to suppress switching frequency instability is limited by its dependence on the nature of load profile. For clarity, the LPF dynamics in the discrete-frequency domain is reported in (12), where τ_{f} is the chosen LPF time constant

$$\mathrm{LPF}(z) = \frac{t_{\mathrm{s}}}{\tau_{\mathrm{f}} z + (t_{\mathrm{s}} - \tau_{\mathrm{f}})}. \tag{12}$$

The sampling time t_{s}, is updated according to the switching frequency $1/f_{\mathrm{sw,min}} \leq t_{\mathrm{s}} \leq 1/f_{\mathrm{sw,max}}$. As such, to see potential effects on the switching frequency oscillations, the LPF time constant should be several orders of magnitude higher than t_{s}, as indicated in Fig. 11 where a Simulink-based simulation has been carried out with indicative time-constant values $\tau_{\mathrm{f}} = 0.25$ ms [see Fig. 11(a)] and $\tau_{\mathrm{f}} = 0.3$ s [see Fig. 11(b)] respectively by introducing, in the model of Fig. 6, an LPF action. However, as shown, the frequency change is reduced and thus the related ATC performance is degraded. Despite an increase in ATC gain K_{ATC} may boost the frequency peak value, it will reintroduce undesired instability oscillations.

III. Proposed Modified SF-ATC Algorithm

From the analysis conducted in Section II it is possible to conclude that, to avoid oscillating switching frequency behavior and instability, two possible solutions are to reduce the ATC gain K_{ATC} or implement an LPF based on option (a) in Fig. 10. However, in this case, the ATC performances in terms of temperature swing reduction are degraded since lower switching frequency variation will be achieved. As such, a possible solution to ensure high ATC effectiveness without abrupt switching frequency oscillations (low K_{ATC}) could be to modify the base active thermal controller in a way to provide stable switching frequency behavior and an amplification of the ATC performance. For this purpose, this work proposes the implementation illustrated in Fig. 12. As shown, in the proposed method the overall variation in the switching frequency f' is obtained based on a modified version of the power losses processing transfer function $F(z)$. The proposed modified ATC strategy operates considering the adoption of a lead-lag network (LLN(z)) in the switching frequency modulation loop. The fundamental idea is to provide a lead action to ensure higher amplification for those load profile cycles with frequency in the region of interests (e.g., for cycles with range from 5 s to c.a. 8 min. duration, 2 mHz $\leq f \leq$ 0.2 Hz) while providing limited effects for higher frequency signals. As such, by introduction of the proposed method, the available switching frequency variation becomes

$$\begin{aligned} \Delta f'_{\mathrm{sw}}(z) &= F'(z) P'_{\mathrm{tot}}(z) \text{ with} \\ F'(z) &= K_{\mathrm{ATC}}\ \mathrm{IHPF}(z)\ z^{-1}\ \mathrm{LLN}(z) \end{aligned} \tag{13}$$

where the introduced lead-lag network LLN(z) transfer function is expressed as

$$\mathrm{LLN}(z) = \frac{\tau'_{\mathrm{f}}\ z + (t_{\mathrm{s}}(1 + k_{\mathrm{sw}}) - \tau'_{\mathrm{f}})}{\tau'_{\mathrm{f}}\ z + (t_{\mathrm{s}} - \tau'_{\mathrm{f}})}. \tag{14}$$

Here, the gain k_{sw} has impact on the offered amplification in the targeted frequency region while τ'_f gives information on the lag action cutoff frequency which will provide the compensation

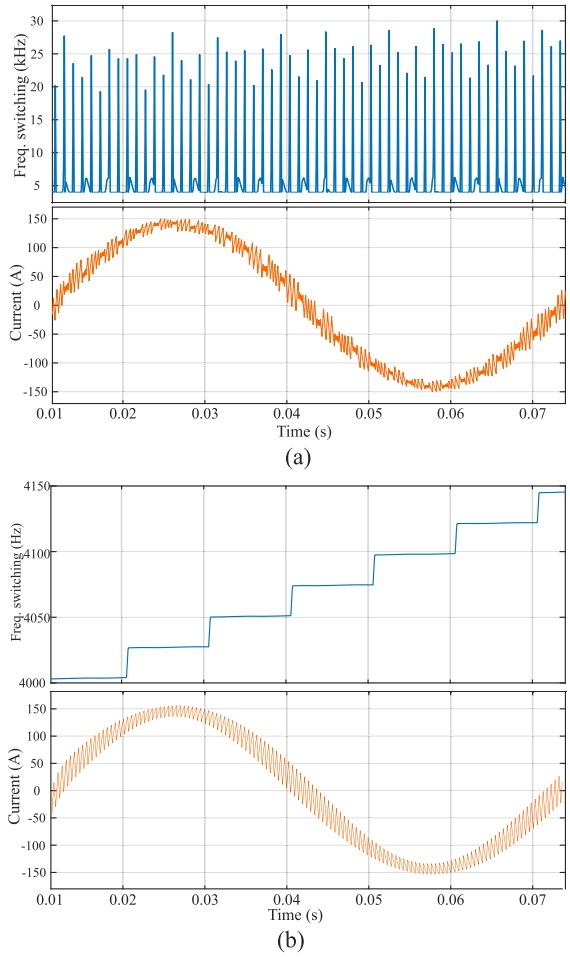

Fig. 8. Analyzed switching frequency instability impact on the system current. In (a) with instability ($K_{\text{tot}} > 1$) and in (b) without instability ($K_{\text{tot}} < 1$).

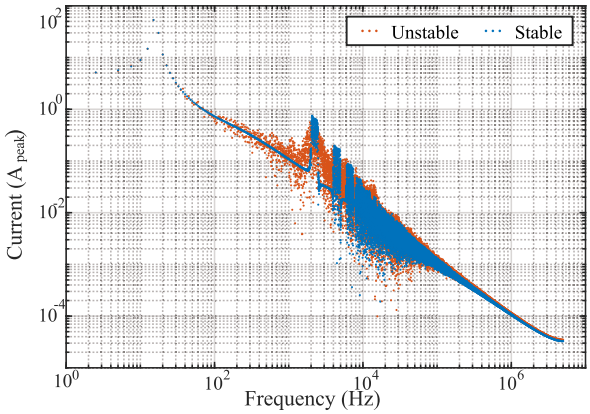

Fig. 9. Unstable switching frequency impact over phase current in frequency domain.

of the lead action for the frequencies outside the region of interest. From the stability point of view, the updated input–output transfer function is reported in

$$f'(z) = \frac{1}{1 - K_{\text{ATC}}\, z^{-1}\, \text{IHPF}(z)\, H(z)\, K_{\text{e,tot}} \text{LLN}(z)}\, f_{\text{n}}. \tag{15}$$

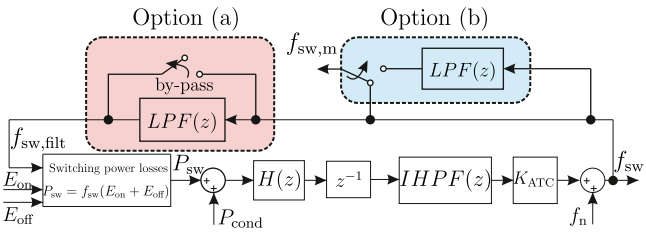

Fig. 10. Switching frequency filtering by means of LPF. In option (a) the LPF is embedded into the modulation loop, whereas in option (b) an external filter is adopted.

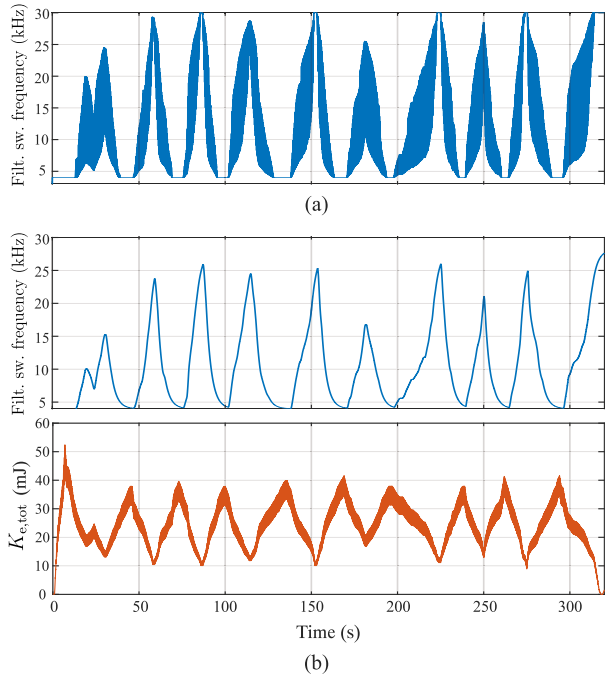

Fig. 11. LPF effects on the switching frequency oscillations, during the instability in simulation. (a) LPF performance when its time-constant is of the same order of the sampling frequency, and (b) for higher time-constant values.

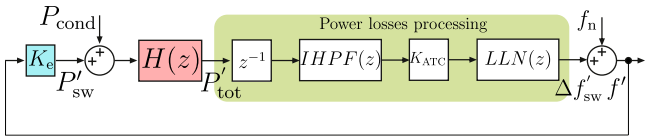

Fig. 12. Proposed LLN-based modification for SF-ATC (single IGBT die).

In a similar way to what has been discussed for the IHPF, the impact of the LLN on the stability of the switching frequency modulation loop can be considered negligible ($\text{LLN}(z) \cong 1$) in the context of the fast dynamics related to the instability phenomenon since $\tau'_{\text{f}} >> t_{\text{s}}$. As a consequence, the gain k_{sw} selection shall be carried out in such a way that the condition $t_{\text{s}}(1 + k_{\text{sw}}) << \tau'_{\text{f}}$ is satisfied.

In order to analyze the effect of $\text{LLN}(z)$ introduction on the system performance, the frequency responses of $F(z)$ and $F'(z)$ are analyzed in Fig. 13. Here, assuming $k_{\text{sw}} = 0.7$ and $\tau'_f = 0.3$ s, different SF-ATC gain values K_{ATC} are selected and the delay action is neglected due to its only effect on the phase shift. As shown, the proposed method provides an

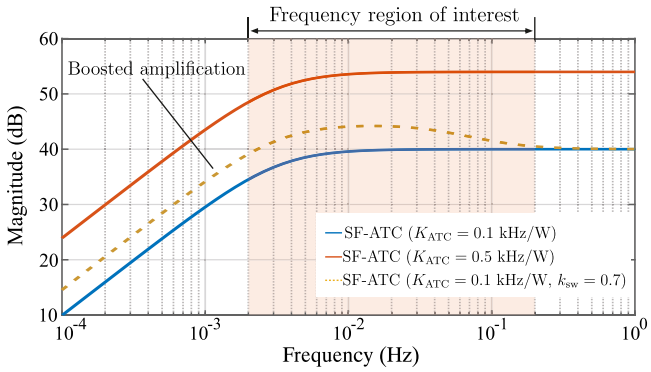

Fig. 13. Frequency response of the base SF-ATC power losses processing transfer function ($F(z)$) and the one for proposed modified active thermal controller $F'(z)$.

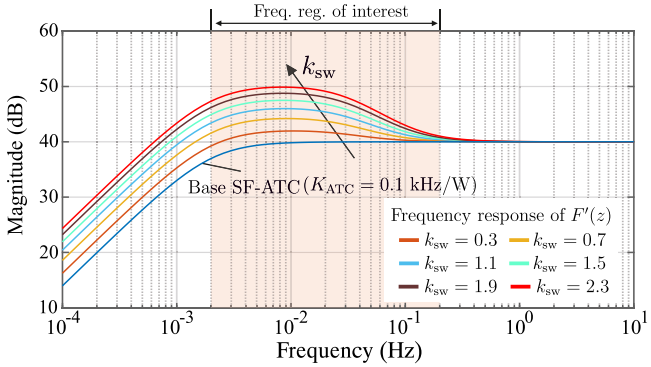

Fig. 14. Frequency response of $F(z)$ and $F'(z)$ with $K_{ATC} = 0.1$ kHz/W and different gain k_{sw} values.

amplification that changes based on the cycles frequency of interest (dashed yellow line). When higher gain K_{ATC} is selected, an up-shift is introduced in the $F(z)$ frequency response thus causing a boosted amplification also for not targeted frequency regions (orange line), leading to high sensitivity to noisy signals.

In contrast, the proposed modified SF-ATC limits the amplification in higher frequency ranges, improving the signal-to-noise ratio of the algorithm. As such, the selection of low K_{ATC} will ensure a stable switching frequency behavior while a proper gain k_{sw} selection will allow to maximize the ATC stress relieving performances.

However, the user should consider that as k_{sw} grows, the boost of amplification in the frequency range of interest tends to reduce (see Fig. 14). Furthermore, using high k_{sw} may increase the amplification, also for cycles outside of the region of interest, further degrading the efficiency. The Simulink-based simulation of the switching frequency dynamics, during the proposed method application, is depicted in Fig. 15.

Here, to ensure a good balance between boost in ATC performance and effective low noise operation, a gain $k_{sw} = 0.7$ and lag-action time-constant $\tau_f' = 0.3$ s have been selected. As demonstrated, the proposed algorithm enables an amplification of the switching frequency variation during each thermal cycle without the occurrence of any abrupt oscillation.

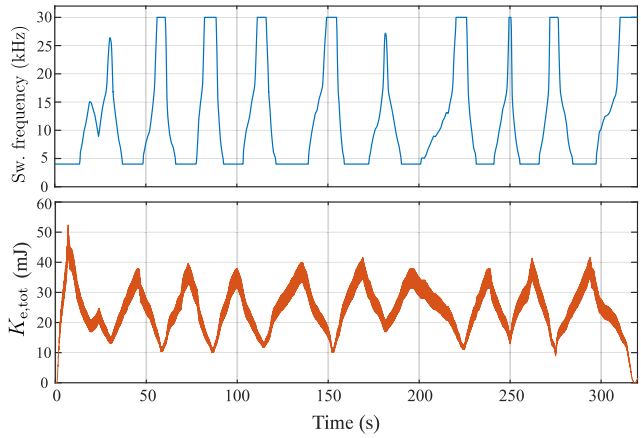

Fig. 15. Proposed method simulation during a generic load mission profile.

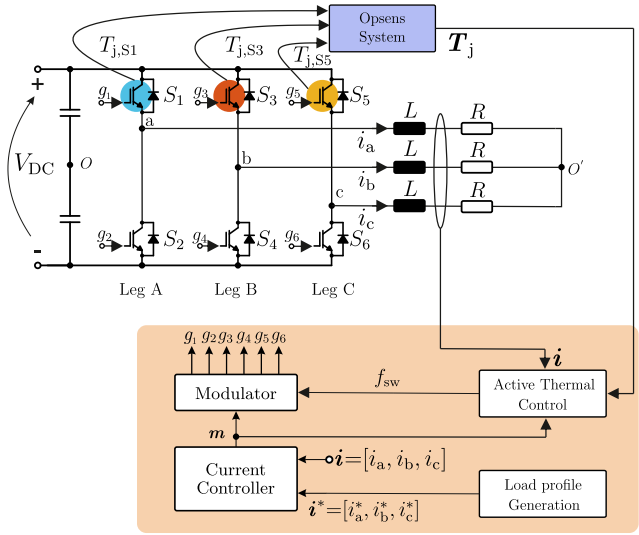

Fig. 16. Three phase test-rig block diagram.

IV. Experimental Results

A. Experimental Test Rig Description

The results presented in this article have been evaluated using a three-phase test rig, the block diagram of which is shown in Fig. 16. The device under test is represented by an Si-IGBT-based two-level voltage source inverter (VSI) with a EconoPIM^{TM}2 -power module of 1200 V/25 A (at $T_{case} = 85°C$)(FP25R12KE3 from Infineon). As in practical implementations, the VSI thermal management is supported by an additional cooling system, an heatsink has been mounted via thermal grease [see Fig. 17(a)] which thermal parameters have been reported in Table II.

The VSI is connected to a three-phase RL load with $L = 0.8$ mH $R = 8.5\,\Omega$ while the dc link voltage is set to $V_{dc} = 450$ V while, as depicted in Fig. 16, the control of the device under

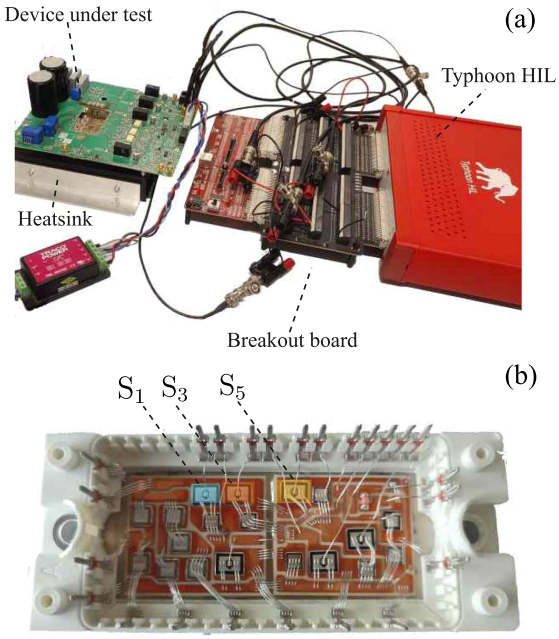

Fig. 17. Three phase test-rig with (a) device under test, HIL interface, and heatsink. (b) Power module under study.

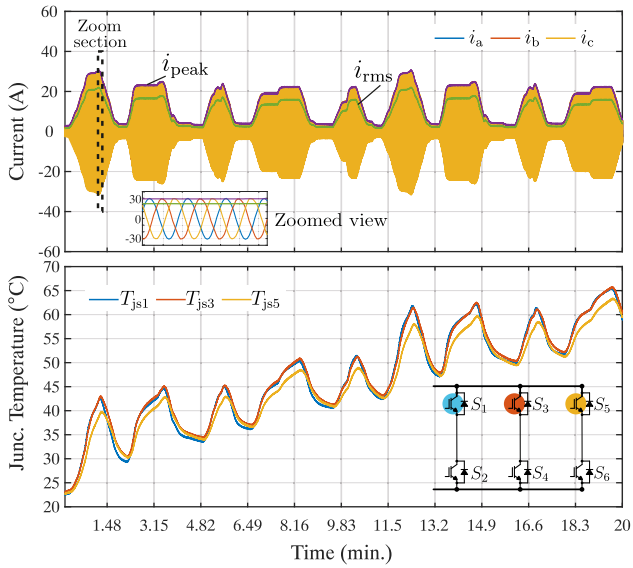

Fig. 18. Applied experimental profile for SF-ATC investigation ($V_{dc} = 450$ V). Three phase current profile (top) and the dies S1, S3, and S5 thermal dynamics (bottom).

TABLE II
DUT AND EXPERIMENT CONDITIONS DATA

Parameter and measure unit	Value
V_{dc}, dc-link voltage (V)	450
I_{max}, max. processed current peak (A)	30
$T_{j,max}$, maximal junction temperature (°C)	150
$f_{sw,max}$, max. switching frequency (kHz)	20
$f_{sw,min}$, min. switching frequency (kHz)	5
N_{hyst}, number of hysteresis steps	5
τ_f, additional LPF time-constant (s)	0.3
k_{sw}, selected modified SF-ATC gain	0.7
R, L, load resistance (Ω) and inductance (mH) value	8.5, 0.8
t_{ATC}, ATC IHPF time-constant (s)	10
R_{hsk}, heatsink therm. resistance (°C/W)	15
C_{hsk}, heatsink therm. capacitance (J/°C)	227

study is obtained by the interface with Typhoon HIL system [see Fig. 17(a)]. In this way, the power flowing from the converter to the load can be varied through its current closed-loop control. In parallel, the modulation depth information $\mathbf{m}$ as well as the load currents $\mathbf{i}$ and die junction temperatures $\boldsymbol{T}_j$ are used in the ATC algorithm. Fig. 17(b) shows the power module under study with its dies allocation. For the purpose of ATC algorithm implementation, the junction temperature of the IGBT dies under investigation are measured using a contact sensor from OpSens solutions (accuracy ±0.3°C and response time of 0.5 s).

B. Experimental Testing Conditions

As mentioned in Section II, not to excessively degrade the converter efficiency, only short-term thermal cycles will be addressed in this analysis. To validate the ATC algorithm effectiveness, a 20-min long modified version of the WLTC profile has been used with T_j-cycling period in the range of minutes.

The analyzed load profile has been implemented based on a repeating sequence of a 6-min long base trajectory which three-phase current $i_{a,b,c}$ as well as its peak and rms value are shown in Fig. 18. Furthermore, the three phase VSI is assumed to work with $V_{dc} = 450$ V, while supplying pure active power (unitary power factor) to the load with nominal frequency $f_g = 50$ Hz. As reported in Fig. 18, dies S1 and S3 present the highest thermal swing as well as instantaneous junction temperature.

In the following, the ATC impact of the cases presented in Sections II and III is evaluated for the chip S3. The impact of potential switching frequency instability on power quality and the ATC performance is presented. Furthermore, a comprehensive analysis of the thermal swing reduction enabled by the use of the proposed method is performed. All the following evaluation have been carried out based on the experimental data in Table II.

C. Base SF-ATC Case

As presented in Section II, the selection of the proper IHPF time constant t_{ATC} and ATC gain K_{ATC} has strong influence on the thermal swing suppression capability of the SF-ATC. This is confirmed in Fig. 19, where the impact of SF-ATC on the die-S3 junction temperature swing for different K_{ATC} values is depicted. In the following, it is assumed to prioritize the damage reduction and the ATC parameters are set to $K_{ATC} = 0.5$ kHz/W and $t_{ATC} = 10$ s as that is combination for achieving the best thermal cycling reduction (see Fig. 3).

Fig. 20 displays the SF-ATC experimental evaluation based on the selected load profile in terms of switching frequency dynamics, averaged S3-die power losses (over one fundamental

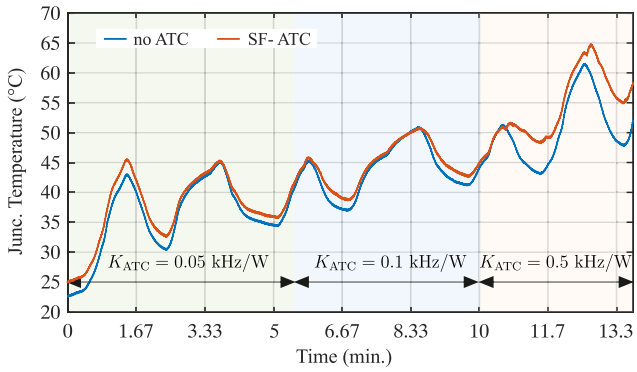

Fig. 19. Experimental evaluation of the impact of different K_{ATC} on thermal swing suppression ($t_{ATC} = 10$ s).

period) and thermal cycling reduction. In particular, Fig. 20(a) presents the thermal cycling reduction obtained when the base SF-ATC is applied. As shown, each thermal swing is suppressed during the ATC operation due to the achieved variation in switching frequency. However, although high reduction is obtainable, the switching frequency exhibits unstable behavior oscillating abruptly between the two selected saturation values. This will negatively impact the stress-relieving operation of the base SF-ATC algorithm due to the introduction of additional peaks in the junction temperature of the die under investigation. The amplitude of these additional peaks reaches up to few degrees for the analyzed case leading to higher damage. In addition, the thermal excursion may enlarge when larger frequency variations are selected. As such, depending on the selected maximal switching frequency for a given application, the instability might reduce ATC effect on thermal swing due to the abrupt increase of the SLPF.

D. Hysteresis and LPF Cases of Study

In Fig. 20(b), the SF-ATC operation is supported by the hysteresis bands application. For the present case of study, a steps number of $N_{hyst} = 5$ is selected in order to provide sufficient noise attenuation. As depicted, the hysteresis band method is not effective in addressing the instability phenomenon and tends to keep an oscillating behavior of the switching frequency hence reducing its effect on T_j-cycling. Similarly, when an internal LPF action is applied in the frequency loop [see Fig. 10, option (a)], the resulting dynamics is shown in Fig. 20(c). An LPF time-constant of $\tau_f = 0.3$ s is chosen to ensure a proper filter action. However, as shown, the filter reduces the switching frequency peak for each thermal cycle which reduces the effectiveness of the ATC algorithm.

E. Proposed Method Validation

In Fig. 20(d), the converter operation is supported by the proposed SF-ATC solution. First, the ATC gain has been reduced to $K_{ATC} = 0.1$ kHz/W, guaranteeing the global loop gain to be sufficiently far from the stability limit. Subsequently, the proposed modification is introduced to increase the SF-ATC effectiveness. As reported, in this case, the provided switching frequency signal f' is obtained based on the selected LLN gain $k_{sw} = 0.7$ and lag-action time-constant $\tau'_f = 0.3$ s. The proposed method provides the maximal available switching frequency variation for all the cycles without abrupt oscillations. Furthermore, in contrast to the case of the hysteresis band method, it allows for a fine compensation of the temperature swing thereby optimizing the damage reduction process (no additional thermal swings are introduced because of the absence of abrupt power loss variation).

F. Impact on the Converter Operation

The experimental evaluation of the impact of the analyzed SF-ATC algorithms and the switching frequency instability on the system power quality can be observed in Fig. 21, that depicts a portion of the three-phase current profile during its descending phase. As illustrated, in the case of the classic high-gain SF-ATC [see Fig. 21(a)] and the SF-ATC with hysteresis band [see Fig. 21(b)], a strong ripple is introduced due to the fast switching frequency oscillations. As a consequence, induced harmonic content (which, in the case of the test-rig under study, has amplitude over 30% of the fundamental component) will be present in the current frequency spectrum during the instability phase (see Fig. 22). However, a power quality improvement is possible if the SF-ATC with an additional LPF [see Fig. 21(c)] or the proposed modified SF-ATC [see Fig. 21(d)] are used as further confirmed by the harmonic analysis in Fig. 22.

G. Evaluation of the Total Damage Reduction and Average Single IGBT Die Power Losses

In this section, the findings of the presented experimental evaluation are discussed in terms of achieved thermal swing and accumulated damage reduction. Fig. 23 presents the junction temperature variation distribution over the selected load profile for the case of no SF-ATC application, the case of classic SF-ATC and the proposed modified controller. Furthermore, to provide metric parameters for the performance comparison, the average thermal swing $(\Sigma\Delta T)_{j,avg}$ experienced on the entire profile is evaluated as

$$(\Sigma\Delta T)_{j,avg} = \frac{\sum_{i=1}^{N_c} \Delta T_{j,i}}{N_c} \tag{16}$$

where N_c stands for the number of half-cycles experienced by the heating-up and cooling down process of the die under study. As depicted, the proposed modified controller is able to provide higher thermal swing reduction with respect to the classic SF-ATC with high gain. Furthermore, the proposed method provides $(\Sigma\Delta T)_{j,avg} \cong 6.9°C$ (44% reduction with respect to the case where no SF-ATC is applied). The total accumulated damage is calculated using the well-established rainflow counting and Coffin–Mason model [26]. The accumulated damage for all the ATCs cases is normalized to the no ATC-case accumulated damage and presented in Fig. 24. The results demonstrate that the proposed method achieves the best thermal stress reduction (by approximately 34%) thanks to the elimination of the additional peaks. Remarkably, despite both the classic SF-ATC

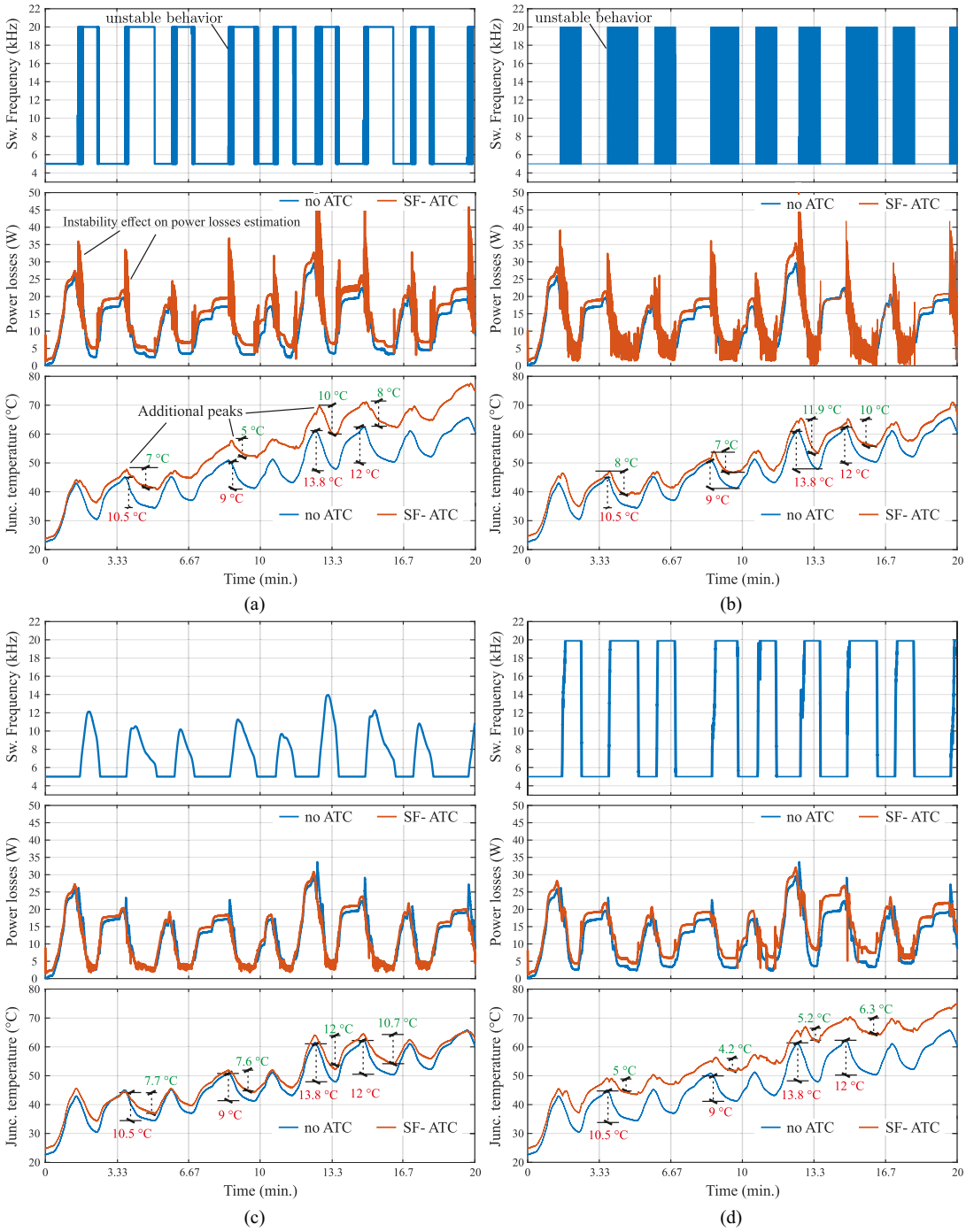

Fig. 20. Experimental evaluation for a single IGBT die operation. (a) Case of the base SF-AT controller with high gain K_{ATC}. (b) Case of the use of an hysteresis band to suppress abrupt f_{sw} oscillations. (c) Case of the use of an additional LPF in the main frequency-modulation loop; and (d) proposed modified SF-AT controller (single IGBT die). (a) SF-ATC (high gain). (b) SF-ATC (hysteresis). (c) SF-ATC (low-pass filter). (d) SF-ATC (proposed strategy).

and the case with hysteresis allow for the maximum switching frequency variation, they will present a damage reduction that is comparable with the one provided by the case of SF-ATC with LPF action. A reason for this is the presence of the additional peaks due to the abrupt change in power losses in the case of the classic SF-ATC and the completely unstable switching frequency variation, in the case of the hysteresis band method application, thus not giving the possibility to effectively reduce the thermal swing.

On the other hand, Fig. 25 shows the impact of the selected SF-ATC strategies on the S3-IGBT die total power losses. For this purpose, the power losses have been integrated over the entire profile duration and have been normalized with respect to the power losses experienced by the IGBT when no ATC is

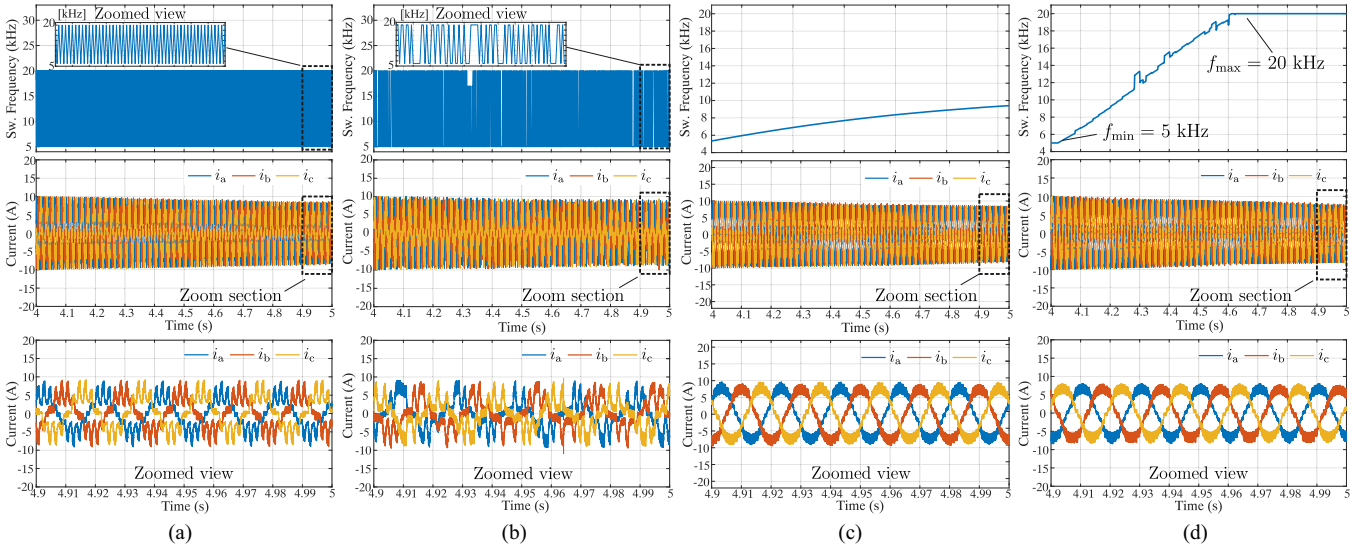

Fig. 21. Experimental evaluation of the impact of the SF-ATC algorithms on the current power quality with zoomed view. (a) SF-ATC (high-gain). (b) SF-ATC (hysteresis). (c) SF-ATC with additional LPF. (d) Proposed modified SF-ATC.

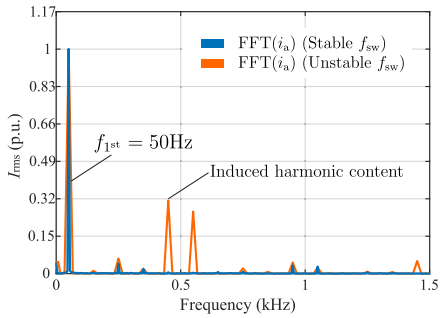

Fig. 22. Impact of switching frequency instability on the phase currents spectrum.

deployed. Interestingly, despite the proposed method presents a notable damage reduction, its impact on the power losses is approximately equal to the one of the SF-ATC with high gain (base SF-ATC). The reason for this is the absence of the additional peaks generated during abrupt variation of the switching frequency during the instability phase during heating-up and cooling-down process of the die. Whereas, as expected, the lowest power losses increase is experienced for the case of the SF-ATC with LPF (c.a. 22 %).

A summary of the experimentally analyzed cases is reported in Fig. 26, confirming that the proposed modification of the SF-ATC provides fine control of the switching frequency without abrupt oscillations and the highest damage reduction at expense of an increase in the die power losses similar to the one for the case of SF-ATC with high gain.

V. Discussion and Future Research Work

The present study investigated the origin, impact and mitigation technique of the switching frequency instability on a three-phase VSI operation. To cope with the problem, a solution based on a modification of the already established SF-ATC was proposed. In general, as highlighted in Section II, the generation of switching frequency instability is experienced when the global loop gain K_{tot} grows over unity. As such, the ATC gain K_{ATC} should be selected to avoid that the overall gain exceeds unity. Then, based on the desired tradeoff between damage reduction and efficiency, the user might adopt the proposed modification or utilize the standard SF-ATC implementation (see Fig. 2).

However, multiple aspects, related to this study, should be further investigated in the future research work such as the following:

- *Sensitivity analysis to model parameters variations:* For the purpose, accelerated cycling aging tests should be carried out on power module under investigation. Subsequently, the effects of the aging on the converter power losses as well as ATC performance should be studied. Furthermore, the statistical relevance of the aging analysis should be increased by testing different power modules.
- *Proposed method impact on EMI:* Additional analysis should be carried out to evaluate the impact of the proposed method on the EMI propagation in practical applications.

It should be further stressed that, as pointed out in different works in the recent research [7], [8], the use of switching frequency to delay the aging of power converters is not suitable for all applications. The applicability of SF-ATC depends on multiple factors such as the following for instance:

1) *Efficiency requirements:* Although a tradeoff between efficiency and SF-ATC effectiveness can be found (see Figs. 3 and 4), there might be applications where the efficiency

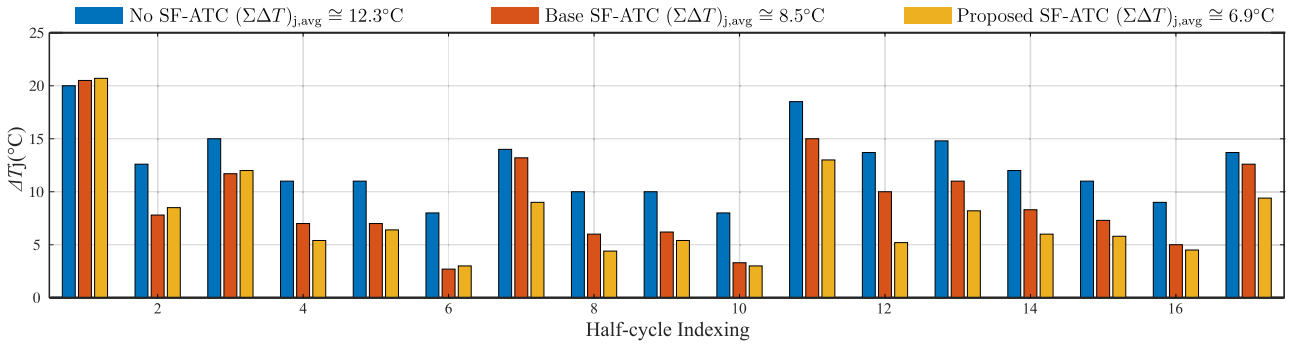

Fig. 23. ΔT_j distribution over the cycles experienced during the analyzed load profile for no ATC, base SF-ATC, and proposed SF-ATC case.

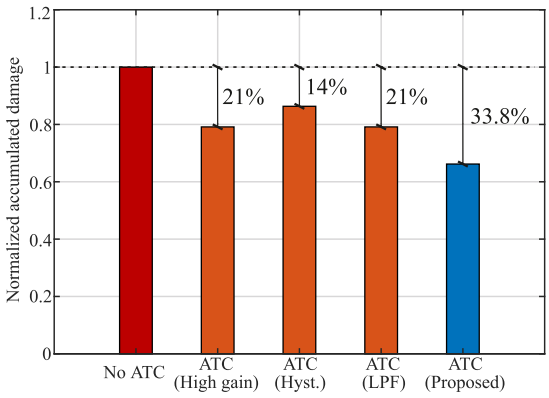

Fig. 24. Accumulated damage comparison among the different analyzed strategies.

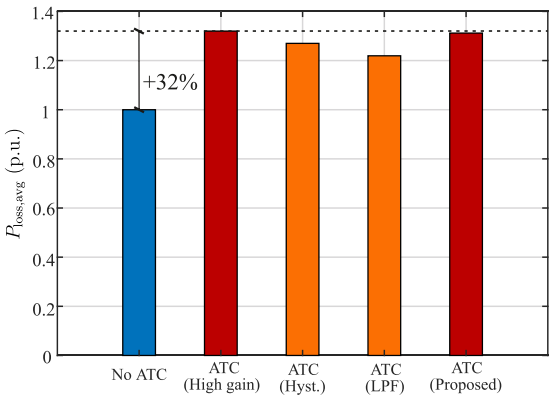

Fig. 25. Impact on a single IGBT die power losses for different ATC strategies.

represents the highest priority. In this case, the use SF-ATC might not be the suitable solution [7], [8].

2) *Selected semiconductor technology:* The type of the selected semiconductor technology can impact the switching losses participation factor that has to be SLPF $\geq 50\,\%$ for being able to influence the temperature dynamics via switching frequency variation.
3) *EMI/power quality:* The SF-ATC designer needs to guarantee the compliance to the standard requirements for EMI/power quality when working with large switching frequency variations [9].

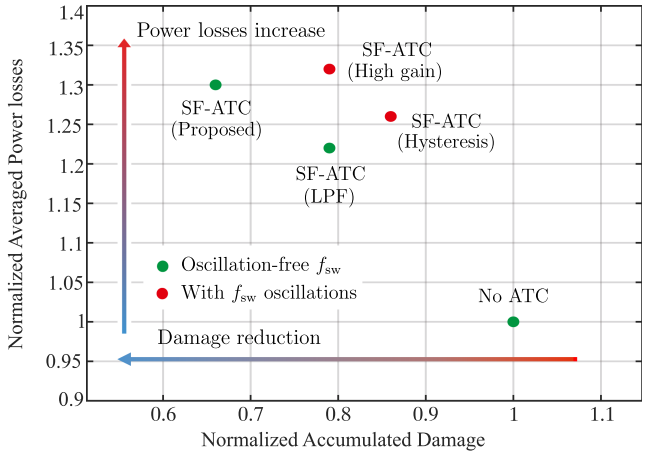

Fig. 26. Impact on a single IGBT dies power losses and accumulated damage for the different ATC strategies.

VI. Conclusion

This study examines switching frequency instability in reference-free SF-ATC strategies and its impact on system performance. The studied instability increases current ripple, noise, and may weaken ATC's thermal stress mitigation. Simulink-based simulations and experiments show that conventional methods, such as hysteresis control and deployment of additional LPF in the switching frequency modulation loop, fail to suppress switching frequency instability oscillations and may reduce ATC's effectiveness. As such, the present work proposed a modified SF-ATC that is obtained by replacing the LPF with an LLN in the switching frequency modulation loop. The LLN selectively amplifies the SF-ATC effect in the relevant thermal cycle frequency range without causing instability. The experimental results, conducted on the converter under test, confirm that this approach eliminates the switching frequency oscillations, triggered by the instability. Furthermore, for the tested converter, adopted load profile and testing conditions, the proposed method leads to an accumulated damage reduction by over 30% as well as an average thermal swing reduction of c.a. 44% compared to the case where no ATC is adopted. However, for the studied case, the SF-ATC thermal swing reduction is obtained at the expenses of an increase of c.a. 32% for the die power losses.

REFERENCES

[1] D. A. Murdock, J. E. R. Torres, J. J. Connors, and R. D. Lorenz, "Active thermal control of power electronic modules," *IEEE Trans. Ind. Appl.*, vol. 42, no. 2, pp. 552–558, Mar./Apr. 2006.

[2] Q. Zhang and P. Zhang, "A junction temperature smoothing control method for SiC MOSFETs based on the gate driving signal delay," *IEEE Trans. Ind. Electron.*, vol. 71, no. 3, pp. 3122–3132, Mar. 2024.

[3] J. Ruthardt, P. Ziegler, M. Fischer, and J. Roth-Stielow, "Model based junction temperature control using the gate driver voltage as a correction variable," in *Proc. 21st Eur. Conf. Power Electron. Appl.*, Genova, Italy, 2019, pp. P.1–P.8.

[4] J. Wölfle, M. Nitzsche, J. Weimer, M. Stempfle, and J. Roth-Stielow, "Temperature control system using a hybrid discontinuous modulation technique to improve the lifetime of IGBT power modules," in *Proc. 18th Eur. Conf. Power Electron. Appl.*, Karlsruhe, Germany, 2016, pp. 1–10.

[5] K. Bu, T. Xu, F. Gao, J. Fang, H. Tian, and W. Lu, "Double-time-Scale active thermal control for single inverter with variable frequency SPWM," in *Proc. IEEE 2nd Int. Power Electron. Appl. Symp.*, Nov. 2023, pp. 1447–1452.

[6] Y. Cao, Y. Peng, C. Zhao, Q. Wang, and Z. Shuai, "Active thermal control with switching frequency modulation for fundamental frequency junction temperature of the VSG," *IEEE Trans. Emerg. Sel. Topics Power Electron.*, vol. 13, no. 1, pp. 531–541, Feb. 2025.

[7] A. Moghassemi, S. M. I. Rahman, G. Ozkan, C. S. Edrington, Z. Zhang, and P. K. Chamarthi, "Power converters coolant: Past, present, future, and a path toward active thermal control in electrified ship power systems," *IEEE Access*, vol. 11, pp. 91620–91659, 2023.

[8] A. Ibrahim, M. Salem, M. Kamarol, M. T. Delgado, and M. K. M. Desa, "Review of active thermal control for power electronics: Potentials, limitations, and future trends," *IEEE Open J. Power Electron.*, vol. 5, pp. 414–435, 2024.

[9] R. Han et al., "Modulated model predictive control for reliability improvement of extremely low frequency power amplifier via junction temperature swing reduction," *IEEE Trans. Ind. Electron.*, vol. 69, no. 1, pp. 302–313, Jan. 2022.

[10] J. Zhang, X. Du, C. Qian, Y. Ye, and J. Zhou, "Design of reference junction temperature swing of power module for thermal management," *IEEE Trans. Power Electron.*, vol. 38, no. 1, pp. 1132–1143, Jan. 2023.

[11] T. A. Polom, B. Wang, and R. D. Lorenz, "Control of junction temperature and its rate of change at thermal boundaries via precise loss manipulation," *IEEE Trans. Ind. Appl.*, vol. 53, no. 5, pp. 4796–4806, Sep./Oct. 2017.

[12] C. H. v. d. Broeck and R. W. D. Doncker, "Active thermal management for enhancing peak-current capability of three-phase inverters," in *Proc. IEEE Energy Convers. Congr. Expo.*, Detroit, MI, USA, 2020, pp. 3312–3319.

[13] C. H. v. d. Broeck, L. A. Ruppert, R. D. Lorenz, and R. W. D. Doncker, "Methodology for active thermal cycle reduction of power electronic modules," *IEEE Trans. Power Electron.*, vol. 34, no. 8, pp. 8213–8229, Aug. 2019.

[14] J. Lemmens, P. Vanassche, and J. Driesen, "Optimal control of traction motor drives under electrothermal constraints," *IEEE J. Emerg. Sel. Topics Power Electron.*, vol. 2, no. 2, pp. 249–263, Jun. 2014.

[15] J. Ruthardt et al., "Closed loop junction temperature control of power transistors for lifetime extension," in *Proc. IEEE Appl. Power Electron. Conf. Expo.*, New Orleans, LA, USA, 2020, pp. 2955–2955, doi: 10.1109/APEC39645.2020.9124000.

[16] J. Ruthardt et al., "Lifetime extension of power semiconductor devices by closed-loop junction temperature control," in *Proc. 2021 23rd Eur. Conf. Power Electron. Appl.*, Ghent, Belgium, 2021, pp. 1–10.

[17] M. Andresen, G. Buticchi, J. Falck, M. Liserre, and O. Muehlfeld, "Active thermal management for a single-phase H-bridge inverter employing switching frequency control," in *Proc. PCIM Europe 2015; Int. Exhib. Conf. Power Electron., Intell. Motion, Renewable Energy Energy Manage.*, Nuremberg, Germany, 2015, pp. 1–8.

[18] T. Xu, F. Gao, and Z. Liu, "Coordinated active thermal control for parallel-connected inverters using global synchronous pulse width modulation," in *Proc. IEEE 9th Int. Power Electron. Motion Cont. Conf.*, Nanjing, China, 2020, pp. 2728–2731.

[19] P. Tan, T. Xu, and F. Gao, "General coordinated active thermal control for parallel-connected inverters with switching frequency control," in *Proc. IEEE 1st Int. Power Electron. Appl. Symp.*, Shanghai, China, 2021, pp. 1–6.

[20] Y. Zhong, Z. Peng, Y. Dai, and H. Xie, "Switching frequency hysteresis junction temperature control strategy for Si IGBT/SiC MOSFET inverter parallel module (SSIPM)," in *Proc. 2023 3rd Int. Conf. Intell. Power Syst.*, Shenzhen, China, 2023, pp. 106–110.

[21] L. Wei, J. McGuire, and R. A. Lukaszewski, "Analysis of PWM frequency control to improve the lifetime of PWM inverter," *IEEE Trans. Ind. Appl.*, vol. 47, no. 2, pp. 922–929, Mar./Apr. 2011.

[22] J. Falck, M. Andresen, and M. Liserre, "Active thermal control of IGBT power electronic converters," in *Proc. 2015-41st Annu. Conf. IEEE Ind. Electron. Soc.*, Yokohama, Japan, 2015, pp. 1–6.

[23] M. Weckert and J. Roth-Stielow, "Chances and limits of a thermal control for a three-phase voltage source inverter in traction applications using permanent magnet synchronous or induction machines," in *Proc. 14th Eur. Conf. Power Electron. Appl.*, Birmingham, U.K., 2011, pp. 1–10.

[24] M. Weckert and J. Roth-Stielow, "Lifetime as a control variable in power electronic systems," in *Proc. Emobility - Elect. Power Train*, Leipzig, Germany, 2010, pp. 1–6.

[25] M. Andresen, M. Schloh, G. Buticchi, and M. Liserre, "Computational light junction temperature estimator for active thermal control," in *Proc. IEEE Energy Convers. Congr. Expo.*, Milwaukee, WI, USA, 2016, pp. 1–7.

[26] S. Rahimpour, H. Tarzamni, N. V. Kurdkandi, O. Husev, D. Vinnikov, and F. Tahami, "An overview of lifetime management of power electronic converters," *IEEE Access*, vol. 10, pp. 109688–109711, 2022.

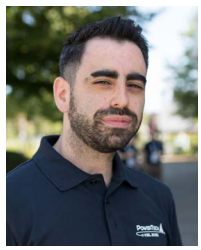

Riccardo Sancio (Student Member, IEEE) received the B.Sc. and M.Sc. degrees in electrical engineering from the Polytechnic of Bari, Bari, Italy, in 2018 and 2021, respectively. He is currently working toward the Ph.D. degree in electrical engineering with the Chair of Power Electronics, University of Kiel, Kiel, Germany.

His research interests include the development of reliability-oriented control solutions for power converters.

Martin Votava received the M.Sc. degree in electrical engineering and the Ph.D. degree in power electronics from the University of West Bohemia, Pilsen, Czech Republic, in 2014 and 2022, respectively.

From 2016 to 2022, he was a Researcher with the Research and Innovation Center for Electrical Engineering, Pilsen, Czech Republic. In 2023, he joined Fraunhofer ISIT, Germany, as a Researcher in power electronics. He is currently a Postdoctoral Researcher with the Chair of Power Electronics, Kiel University, Kiel, Germany. His research interests include multiport converters, thermal modeling, digital twin technology, and condition monitoring of power converters.

Karthik Debbadi (Student Member, IEEE) received the M.Sc. degree in electrical power engineering from RWTH Aachen University, Aachen, Germany, in 2016. He is currently working toward the Ph.D. degree focusing on the reliability of wide bandgap devices in power electronic applications with the Chair of Power Electronics, Kiel University, Kiel, Germany.

He was a Research Scientist in the field of power electronics with United Technologies Research Center, Cork, Ireland. He is currently a Scientific Employee in the field of reliability with the Fraunhofer Institute for Silicon Technology, Itzehoe, Germany. His research interests include reliability of power electronics, active thermal control, thermal modeling, and wide bandgap-based device applications in electric drives.

Yoann Pascal received the engineering degree from École polytechnique, Paris, France, in 2015, the M.Sc. degree in electrical engineering from KTH, Stokholm, Sweden, in 2016, and the Ph.D. degree in electrical engineering from École normale supérieure Paris-Saclay Gif-sur-Yvette, France, in 2019.

His Ph.D. research was focused on PCB-embedding of power electronics dies and magnetic components, with focus on parasitics and reliability. From 2020 to 2022, he was a Postdoctoral Researcher with the Chair of Power electronics, Kiel University, Kiel, Germany. From 2020 to 2022, he was a Postdoctoral Researcher with the Chair of Power electronics, Kiel University. Since 2025, he has been a Head of the Electronic Energy Systems Group, Fraunhofer Institute for Silicon Technology ISIT, Kiel, Germany, which he joined in 2022. His research interests include condition monitoring, and active thermal control, as well as dc–dc power conversion (multiport converters, industrial inverter).

Marco Liserre (Fellow, IEEE) received the M.Sc. and Ph.D. degrees in electrical engineering from the Politecnico di Bari, Bari, Italy, in 1998 and 2002, respectively.

Since 2012, he has been Associate Professor with the Politecnico di Bari and a Professor of reliable power electronics with Aalborg University, Aalborg, Denmark. Since 2013, he has been a Full Professor and holds the Chair of Power Electronics with the University of Kiel, Kiel, Germany. He has been offered and declined professorships at several universities. He has authored or coauthored more than 700 technical papers (1/3 of them in international refereed journals), one book, and seven granted patents (four with companies). These works have received more than 50 000 citations. From 2014 to 2021, he was selected as a Highly Cited Researcher in the field of Engineering (Clarivate Web of Science). Several of his students (M.Sc., Ph.D. and Post-docs) are in leading positions in industry and universities worldwide. In 2023, he joined the Fraunhofer ISIT on a part-time basis as Deputy Director and Director of the new division "Electronic Energy Systems," as well as of the Kiel branch of the Fraunhofer ISIT. He is currently the Acting Director with Fraunhofer ISIT.

Dr. Liserre is a Member of IAS, PELS, PES, and IES. He has served all these societies in various capacities. In PELS, he is a Co-Editor of the IEEE OPEN ACCESS JOURNAL IN POWER ELECTRONICS and Technical Committee Chairman of the Committee on Electronic Power Grid Systems. He has Co-Chaired several IEEE conferences being several times Chairman. He was the recipient of 16 awards from IEEE, PCIM, and EPE-PEMC, including the prestigious 2018 IEEE-IES Mittelmann Achievement Award and the 2023 IEEE-PELS R. David Middlebrook Achievement Award. In 2023, he was the recipient of the title of "Ufficiale" by the President of the Italian Republic. In 2025, he will be Chairman of Powertech 2025 in Kiel.